Amino Acids (2014) 46:449–457
DOI 10.1007/s00726-013-1638-2

ORIGINAL ARTICLE

Design, synthesis, and in vitro evaluation of a binary targeting MRI contrast agent for imaging tumor cells

Yuping Yang · Jinlan Zhou · Kaichao Yu

Received: 5 April 2013 / Accepted: 7 December 2013 / Published online: 12 January 2014

Abstract A binary targeting vector that consists of peptide sequences of Arg-Gly-Asp (RGD) and Asn-Gly-Arg (NGR) motifs has been designed and synthesized using solid-phase peptide synthesis procedure. The vector is then coupled with Gd-DOTA to work as a targeting contrast agent (**CA1**) for magnetic resonance imaging of human lung adenocarcinoma cells A549. Its longitudinal relaxivity is measured to be 7.55 mM^{-1} s^{-1} in aqueous solution at a magnetic field of 11.7 T, which is higher than that of Magnevist (4.25 mM^{-1} s^{-1}) in the same conditions. The cell experiment shows, at the same concentration, uptake quantity of **CA1** by A549 is much more than Magnevist and also superior over **CA2** (a single targeting contrast agent contains only RGD). The uptake can be blocked by the targetable peptide containing RGD or NGR without coupling Gd. To summarize, **CA1** has very good ability to target A549 and higher relaxivity than that of Magnevist. So **CA1** is promising MRI contrast agent for high-resolution MR molecular imaging of human lung adenocarcinoma A549 cells.

Keywords MRI contrast agent · Tumor-targeted · Binary vector of peptide sequence · Gd-DOTA

Electronic supplementary material The online version of this article (doi:10.1007/s00726-013-1638-2) contains supplementary material, which is available to authorized users.

Y. Yang · J. Zhou · K. Yu (✉)
School of Chemistry and Chemical Engineering, Huazhong University of Science and Technology, Wuhan 430074, Hubei, People's Republic of China
e-mail: yukc@163.com

Y. Yang
e-mail: yyp.cc@163.com

Introduction

Medical imaging has significance for both disease diagnosis and therapeutic efficacy assessment; many imaging modalities were developed for these purposes. In this regard, magnetic resonance imaging (MRI) is superior over other imaging modalities due to its noninvasiveness, non-ionizing radiation, and high spatial and temporal resolution (Seward et al. 2008; Ye et al. 2008). However, its application suffers from a serious drawback of low sensitivity. Use of targeted contrast agent is the method of choice to increase imaging sensitivity. Different strategies have been developed to improve the performance of Gd-based agents (Heverhagen et al. 2004; Caravan 2009). It is found that when Gd-chelate is covalently or noncovalently linked to macromolecule substrates, such as dendrimers (Nwe et al. 2010; Langereis et al. 2007), chitosan oligosaccharide (Huang et al. 2013), and ploy-peptides (Caravan 2009; Schroeder et al. 2011), the tumbling rate of the molecule will slow down and the relaxivity of Gd-chelate dramatically improve. In this arena, Gd-chelate-peptide derivatives get more attention because of their good biocompatibility and high binding affinities to their targets (Langereis et al. 2005; De León-Rodríguez and Kovacs 2008).

Peptide-based targeting vectors are becoming increasingly popular for both diagnostic and therapeutic applications (Li and Cho 2012; Ndinguri et al. 2009; Mishra et al. 2009). One of its advantages is the combination of multiple peptide sequences which can increase binding affinity to its target (Dijkgraaf et al. 2006, 2007; Liu et al. 2009). For example, Dijkgraaf et al. synthesized monomer, dimmer, and tetramer of Arg-Gly-Asp (RGD) motifs conjugated to ^{111}In-DOTA and investigated their binding affinities to the integrin $\alpha_v\beta_3$. The results revealed that multimeric RGD

peptides enhance the binding affinity to the $\alpha_v\beta_3$ integrin (Dijkgraaf et al. 2006, 2007). But limited number of $\alpha_v\beta_3$ could be available, as restrict the highest binding concentration of RGD to tumor cells. A binary targeting vector including two different targeting motifs (RGD and NGR), which can bind with two different biomarkers of tumor cells, will improve tremendously the binding amount to tumor cells. Based on the assumption, we designed and synthesized a binary targeting vector including Arg-Gly-Asp (RGD) and Asn-Gly-Arg (NGR) motifs. RGD peptide is prone to combine specifically with the $\alpha_v\beta_3$ integrin (Hersel et al. 2003); NGR peptide specifically recognizes aminopeptidase N (CD_{13}) receptor (Wang et al. 2011; Soudy et al. 2012). As is well known, $\alpha_v\beta_3$ and CD_{13} are two kinds of biomarkers of tumor cells. The binary targeting MRI contrast agent (**CA1**) can bind with not only $\alpha_v\beta_3$ but also CD_{13}. So, to tumor that express both $\alpha_v\beta_3$ and CD_{13}, **CA1** can improve MRI sensitivity.

In the present study, our main aim is to design and synthesize a binary targeting contrast agent KFDGRGK(Gd-DOTA)GGCNGRC (**CA1**) including two targeting motifs of RGD and NGR and a single targeting contrast agent (**CA2**) including only one targeting motifs of RGD. Then using non-targeting contrast agent Magnevist (a contrast agent commonly clinical used) and KFDGRGK(Gd-DOTA) (**CA2**) as the control agent, on the A549 cells, investigates the targeting performance of the binary contrast agent **CA1**. Peptide KFDGRGKGGCNGRC (**P1**) and KFDGRG (**P2**) were also synthesized. Using **P1** and **P2** as the blocking agent, the binding specificity of **CA1** was investigated.

There are lots of reports on the application of RGD and NGR for both drug delivery and molecular imaging (Conradi et al. 2012; Ma et al. 2013). However, there is still no report on combining RGD with NGR to become a more effective targeting molecular. So a success experiment result will be meaningful to therapy and diagnosis of tumor.

Experimental

Materials and methods

N,*N*-Diisopropylethylamine (DIPEA), 1-hydroxybenzotriazole (HOBt), *N*,*N*,*N*′,*N*′-tetramethyl-*O*-(1H-benzotriazol-1-yl) uronium hexafluorophosphate (HBTU), trifluoroacetic acid (TFA), all protection amino acids, and Rink Amide-MBHA resin (0.54 mmol/g loading) were all purchased from GL Biochem (Shanghai, China) Ltd. and used without further purification. Human lung adenocarcinoma epithelial cells (A549) used in this work were obtained from Cell Bank for Division of Nanobiomedicine, Suzhou Institute of Nanotech and Nanobionics, Chinese Academy of Sciences (Suzhou, China). DMEM culture medium and fetal bovine serum were purchased from Invitrogen (agency in Shanghai, China). Magnevist was purchased from Guangzhou consun Pharmaceutical Co., Ltd (Guangzhou, China). All other reagents were of analytical grade and used as received, Utrapure water (18.2 MΩ cm^{-1}) was used in all experiments.

Purification of peptides and ligands was performed on semi-preparative reverse-phase HPLC (LC-6AD Shimadzu, Japan) with a C-18 column (250 × 21.4 mm, 100 Å/5 μm). Purity Analytical reversed phase HPLC was performed on the same instrument with a C-18 Microsorb column (4.6 × 250 mm, 100 Å/5 μm) and eluted with a linear gradient of 0–60 % CH_3CN-H_2O in 0.1 % aqueous TFA in 30 min. The HPLC system is coupled to a UV/Vis detector probing at 220 nm. Molecular weight of the products were determined by high-resolution electrospray ionization mass spectrometry (HRESI-MS Agilent Technologies 6220 Accurate-Mass TOF LC/MS, Santa Clara, USA).

Gadolinium content in solution containing contrast agent was measured by inductively coupled plasma atomic emission spectroscopy (ICP-AES, PerkinElemer Optima 8000, PE, America).

Longitudinal relaxivity (r_1) measurements and MRI experiments were conducted on a Bruker 500WB spectrometer (Bruker NMR, Germany) with an 89-mm vertical-bore magnet of 11.7 T using a 15-mm-i.d. coil.

A549 cells were cultivated in recommended medium DMEM with 10 units/mL penicillin, 10 μg/mL streptomycin and supplemented with fetal bovine serum (FBS) at a concentration of 10 %. All media, serum and antibiotics were provided by Invitrogen Life Technologies (Carlsbad, CA, USA). Cell cultures were performed in a 5 % CO2 atmosphere at 37 °C and 95 % humidity within a ThermoFisher Scientific (Rockford, IL, USA) 3111 incubator.

Synthesis of 1,4,7-Tri-Boc-10-(carboxymethyl)-1,4,7,10-tetraazacyclododecane (**DOTA(tBu)$_3$**)

DOTA(tBu)$_3$ was prepared by a multistep synthesis procedure starting from cyclen hydrochloric salt. The synthetic procedure is outlined in Fig. 1. For a detailed statement of the procedure see supporting information.

Synthesis of peptide KFDGRGKGGCNGRC (**P1**)

P1 was manually prepared by a standard *N*-α-9-Fluorenylmethoxycarbonyl (Fmoc) peptide synthesis strategy

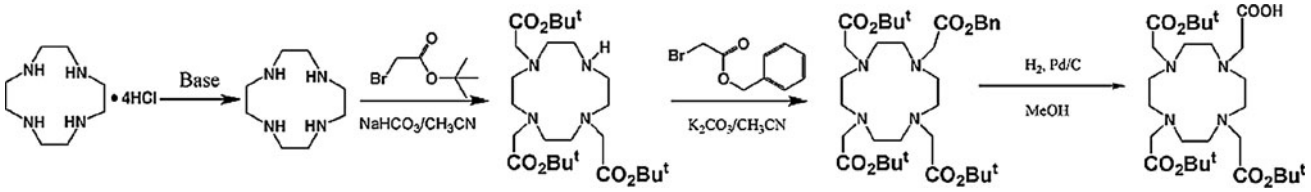

Fig. 1 Synthesis of 1,4,7-Tri-Boc-10-(carboxymethyl)-1,4,7,10-tetraazacyclododecane

using Rink Amide MBHA resin as the solid support. The resin was swelled in DMF for 1 h, and then according to the designed amino acid sequence, all kinds of protected amino acids (Fmoc-Lys(Boc)-OH, Fmoc-D-Phe-OH, Fmoc-Asp(otBu)-OH, Fmoc-Gly-OH, Fmoc-Arg(pbf)-OH, Fmoc-Gly-OH, Fmoc-Lys(Boc)-OH Fmoc-Gly-OH, Fmoc-Gly-OH, Fmoc-Cys(Acm)-OH, Fmoc-Asn(Trt)-OH, Fmoc-Gly-OH, Fmoc-Arg(pbf)-OH, Fmoc-Cys(Acm)-OH) were taken one by one to proceed with the cyclical steps of Fmoc deprotection (20 % v/v piperidinein DMF) 5 × 2 min, washing (DMF, 5 × 3 min) and backbone elongation (coupling). The backbone elongation was activated by HBTU, HOBt, and DIPEA(*N*,*N*′-Diisopropylethylamine) (2 h). The coupling reaction used a threefold excess of amino acid to resin. 1 equivalent of HBTU and HOBt, 2 equivalent DIPEA. The coupling efficiency (>99 %) in every coupling step was determined by measuring residual free amine with quantitative ninhydrin assay (Sarin et al. 1981). The coupling stage was repeated twice for the attachment of the first amino acid to resin. After elongation and final Fmoc deprotection, the intramolecular disulfide bond was formed between the two cysteine residues. The solution of 5 M I_2 in DMF was added into the reacting system stirring for 3 h to remove the side-protection group Acm of Cys (Acm)-OH and simultaneity to oxidize the two sulfhydryl to form a disulfide bridge. Excessive iodine was removed with sodium thiosulphate ($Na_2S_2O_3{\cdot}5H_2O$, aq). Then the resin was washed with 3 × 2 mL DMF, 3 × 2 mL DCM, and 3 × 1 mL MeOH; then the crude peptide was cleaved from the Rink Amide MBHA resin by treatment with a mixture solution of 90 % TFA, 2 % p-cresol, 5 % thioanisole, and 3 % ethanedithiol for 4 h at 0 °C. Meanwhile, all the other protective groups were removed. The supernatant was displaced through filtration into a 10-mL centrifuge tube and the combined washed with a further 1 mL TFA. The combined washings were treated with ~10 mL cold Et_2O to precipitate the peptides. The solids were pelleted by centrifugation for 15 min at 3,000 rpm and washed repeatedly in cold Et_2O (three times in total). The sediment was collected and dissolved in water and were purified by semi-preparative RP-HPLC over a gradient of MeCN in 10 mM NH_4OAc pH 5.2 MeCN). Detection was by UV absorbance at 220 nm. The product was obtained by lyophilisation as a white amorphous solid. Purity of L1 was 98 % as determined by analytical HPLC. Retention time is 3.93 min. see Fig. 2a. *m/z* (HRESI-MS+), 1,451.6740 ($[M+H]^+$), 726.3436 ($[M+2H]^{2+}$), 484.5666 ($[M + 3H]^{3+}$), see Fig. 3a.

Synthesis of peptide KFDGRG (**P2**)

The peptide **P2** was synthesized according to the procedure for **P1**. However it has no cyclization process because it is a line peptide. The peptide was elongated and washed, and cleaved and purified as detailed above. The produce was recovered by lyophilisation as a white amorphous solid. HPLC retention time 7.439 min. *m/z* (HRESI-MS+), 678.3644 ($[M+H]^+$), see the support information figure S6:b and figure S7:b.

Synthesis of ligand KFDGRGK(-DOTA)GGCNGRC (**L1**)

The (**L1**) was prepared as for P1. Except for the middle *N*-Fmoc-Lys(tBu)-OH was changed to *N*-Fmoc-Lys (Dde)-OH and *N*-Fmoc-Lys (Dde)-OH was selected as an anchoring site to conjugate with $DOTA(tBu)_3$ with 2 % hydrazine monohydrate in DMF (25 mL/g) at rt for 3 min. The reaction of $DOTA(tBu)_3$ with middle Lys was completed in the similar manner as other amino acids was coupled. HPLC retention time is 9.463 min. See Fig. 2b. *m/z* (HRESI-MS+), 1,838.8541 ($[M+H]^+$), 919.4332 ($[M+2H]^{2+}$), 613.2926 ($[M+3H]^{3+}$), 460.2227 ($[M+4H]^{4+}$). See Fig. 3b.

Synthesis of ligand KFDGRGK(-DOTA) (**L2**)

The (**L2**) was prepared as for **L1**. HPLC retention time was 13.273 min. *m/z* (HRESI-MS+), 1,192.6407 ($[M+H]^+$), 596.8277 ([$[M+2H]^{2+}$]), 398.2219 ($[M + 3H]^{3+}$), see the supporting information in Figures S8:b and S9:b.

Gadolinium complex KFDGRGK(Gd-DOTA)GGCNGRC (**CA1**)

L1 was dissolved in demineralised water. The pH of the aqueous solution was adjusted to 6.5–7.0 by adding small aliquots of 0.25 % NaOH (aq). Subsequently, a solution of gadolinium chloride hexahydrate (0.99 equiv.) in water

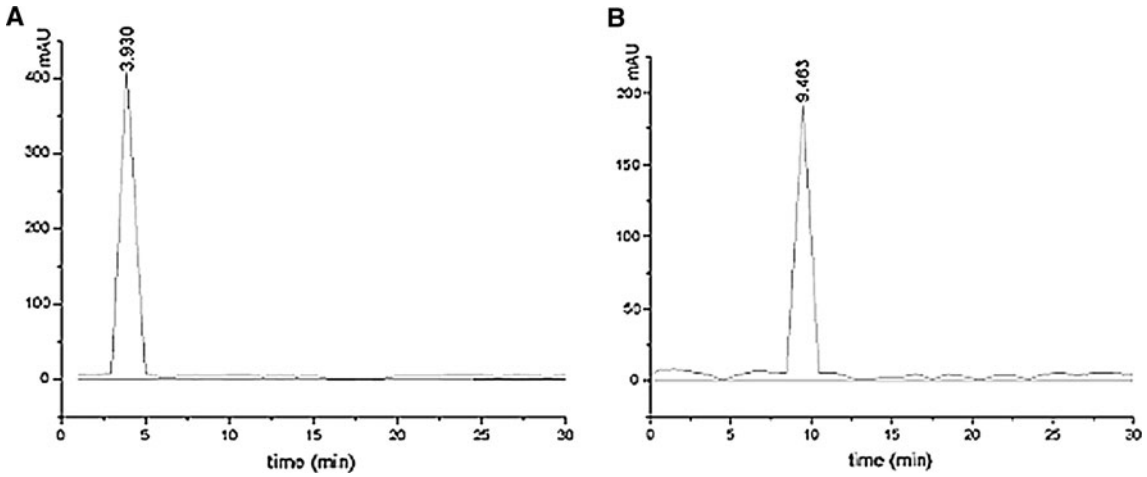

Fig. 2 **a** HPLC eluting chart of **P1**; **b** HPLC eluting chart of **L1**. Eluted with a linear gradient of aqueous CH_3CN (0–60 %, 30 min) solution containing 0.1 % (v/v) TFA and detected by UV absorbance at 220 nm

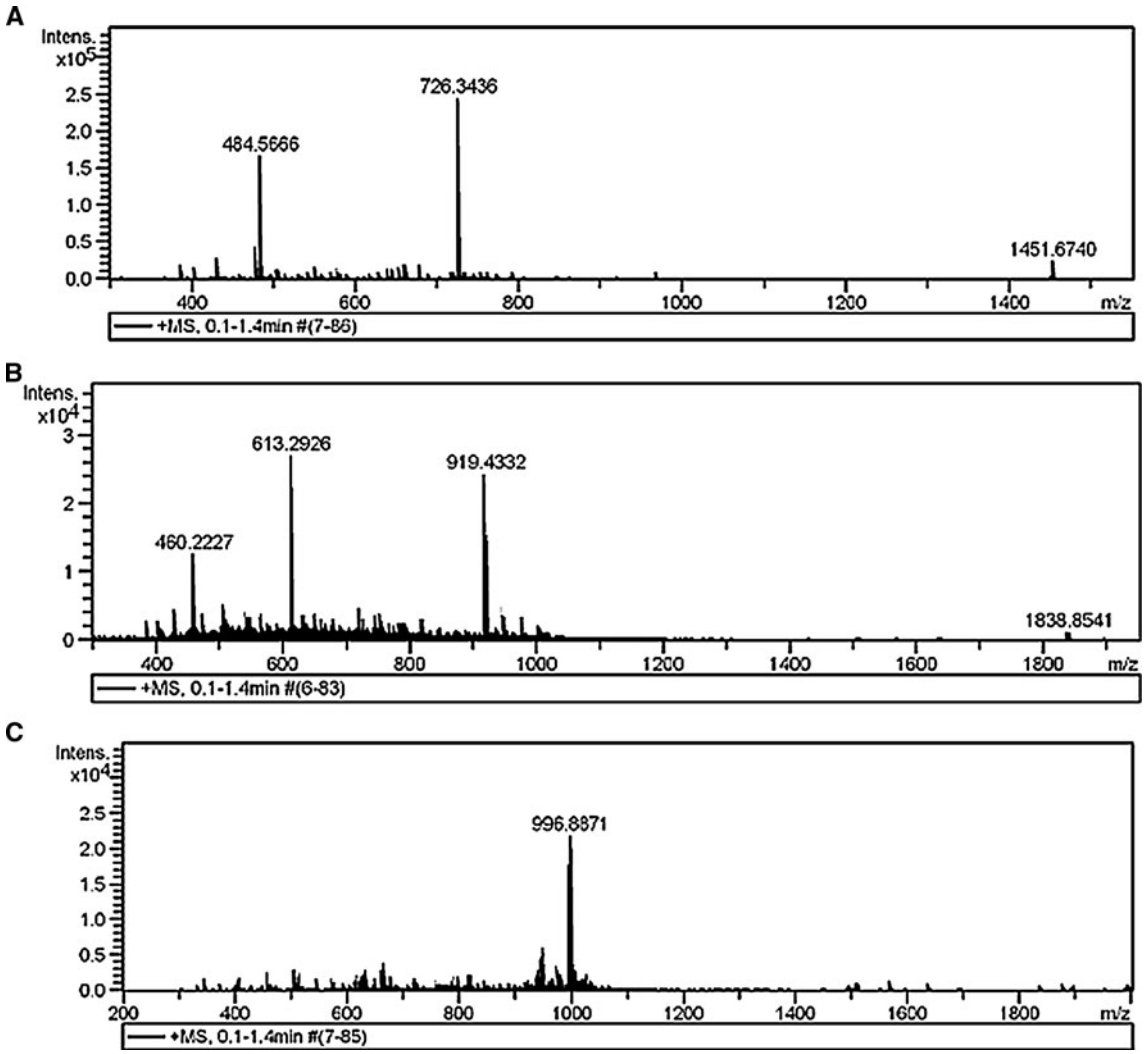

Fig. 3 **a** The mass spectrometry of **P1**; **b** the mass spectrometry of **L1**; **c** the mass spectrometry of **CA1**

was added to the above reaction bottle. The mixture was vigorously stirred for 4 h at room temperature and pH of the reaction system was kept at 6.5–7.0 by adding 0.25 % NaOH (aq) solution. The crude product was purified by dialysis bag. Then condensed and lyophilized to get gadolinium complex **CA1** as white hygroscopic powder (yield 94.65 %). Figure 4 is the structure chart of **CA1**. Gd content was measured by ICP-AES. The observed value of gadolinium content was 94.5 % of the theoretical value. *m/z*, 996.8871 ([[M+2H]$^{2+}$]), see Fig. 3c.

Gadolinium complex KFDGRGK(Gd-DOTA) (**CA2**)

The **CA2** was prepared in the same manner as that for **CA1**. Supporting information Figure S10:b is the structure chart of CA2. Gd content is 97.6 % of the theoretical value measured by ICP-AES. *m/z* 1,347.5453 ([[M+2H]$^{2+}$]), 674.2812 ([[M+2H]$^{2+}$]), see the supporting information in Figure S11:b.

Relaxivity measurements and phantom experiment

To determine the longitudinal relaxivity (r_1), seven different concentrations of the three contrast agents (**CA1,CA2** and Magnevist), respectively (0, 0.05, 0.1, 0.2, 0.4, 0.8, 1.2 mM), were prepared. Relaxation time (T_1) of these solutions was measured on a Bruker AVANCE III500WB Spectrometer and a linear 15-mm-i.d birdcage coil was used for radiofrequency transmission and signal reception. r_1 (mM^{-1} s^{-1}) was calculated through linear fitting of the reciprocal of the T_1 relaxation time versus the gadolinium concentration (mM). T_1-weighted images of all solution were acquired by Multi-Slice Multi-Echo imaging sequence using inversion times of 50, 100, 200, 400, 700, 1,400, 2,000, and 2,800 ms, an echo time (TE) of 6 ms, and an echo train length of 8 at a repeat time (TR) of 300 ms, with a 20 × 15 cm field of view (FOV), 3 mm slice thinness, 125 × 125 × 125 matrix, and one excitation.

Targeting efficiency measurement

A549 cells (5 × 10^5 cells/well) were seeded in 24-well culture plates and cultured overnight to allow the cells to adhere to the plate wall. Then cells were divided into three groups (group 1, group 2, group 3): group 1 was incubated with **CA1** for 8 h, including eight different concentrations (0.05–1.2 mM); every concentration is in triplicate. Using the same method, group 2 was incubated with **CA2**, and group 3 with Magnevist. Following incubation, the nutrient solution was wiped off, and the cells were washed twice with phosphate-buffered saline (PBS) to remove unbound Gd complex. Gd content presented in the cells was determined by ICP-AEP spectrometer. The result was described as mean ± SD.

Binding competition measurement

A549 cells (5 × 10^6 cells/well) were seeded in 24-well culture plates and were cultured overnight to allow the cells to adhere to the plate wall; then the cells were divided into three groups (group 1, group 2 and group 3) and every group contained three parallel samples. First, groups 2 and 3 were cultured with 0.8 mM **P2**, 0.8 mM **P1**, respectively, for 2 h. After that, the three groups were simultaneously cultured with 0.8 mM **CA1** for 8 h. Cells then were washed twice with phosphate-buffered saline (PBS) to remove unbound **CA1**, **P1**, and **P2**. Gd content presented in the cells was determined by ICP-AES; then all three samples were fixed by 1 % agarose and then imaged with a 11.7 T NMR spectrometer. The imaging condition is as above.

Statistical analysis

Analysis of variance and Student's *t* test were used to analyze the data. The level of significance in all statistical

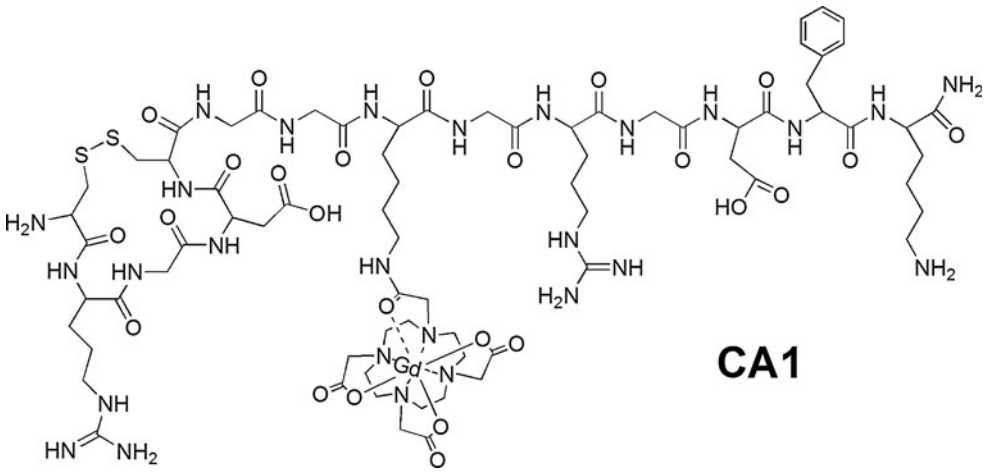

Fig. 4 The structure chart of **CA1**

analyses was set at a probability of $p < 0.05$. Data were described as mean ± SD.

Results

Syntheses and characterization of the products

The ligands (**L1** and **L2**) and peptides (**P1** and **P2**) were assembled using manual solid-phase Fmoc peptide chemistry (Kates et al. 1993). The **L1** and **L2** were conjugated with Gd to work as the contrast agent **CA1** and **CA2**, the **CA1** included two targeting motifs of RGD and NGR binding to $\alpha_v\beta_3$ and CD_{13}, respectively, and the **CA2** included only one targeting motif of RGD binding to $\alpha_v\beta_3$. The **P1** and **P2** were prepared for the competition binding experiments and the **CA2** for comparing targeting effect with the binary targeting contrast agent **CA1**.

The purity assay of the all products was carried out by analytical HLPC, The purity of each product was more than 90 %, (see Fig. 2). Chemical characterization of all products was confirmed by high-resolution electrospray ion mass spectrometry. Found values of Mass spectrometry of all products were consistent with their theoretical values. (see Fig. 3). The content of gadolinium was determined by ICP-AES. Coordination efficiency of Gd is more than 90 %.

Relaxivity and Phantom

The relaxivity (r_1) is 7.55 mM^{-1} s^{-1} for **CA1**, 6.36 mM^{-1} s^{-1} for **CA2,** and 4.25 mM^{-1} s^{-1} for Magnevist (Fig. 5a). r_1 of the **CA1** is much higher than r_1 of Magnevist and **CA2**. Comparing with Magnevist, **CA1** has better imaging effect. From Fig. 5b, it is clear that the imaging of **CA1** is significantly brighter than the imaging of Magnevist under the same concentrations. Even the imaging brightness of **CA1** at the concentration of 0.05 mM is equivalent to that of Magnevist at the concentration of 0.8 mM.

Targeting effect comparison

Comparing the quantity of **CA1**, **CA2**, and magnevist absorbed by A549, from Fig. 6, we can see the quantity of **CA1** combined with A549 is far more than that of Magnevist combined with the cells at the same concentration of Gd, and also superior over **CA2** at the same concentration ($p < 0.01$, **CA1** versus Magnevist $p < 0.01$, **CA2** versus Magnevist 0.4–1.2 mM, $p < 0.05$, **CA1** versus **CA2**). The combined quantity of **CA1** reached saturation at the concentration of 0.8 mM. The combined quantity of **CA2** reached saturation at the concentration of 1.0 mM. It reveals that two targeting moieties result in higher concentration of the contrast agent to the surface of the tumor and better imaging effect.

Competition binding

The result of competitive binding is showed in the Fig. 7a, **P2** included the sole targetable-tumor motif of RGD can

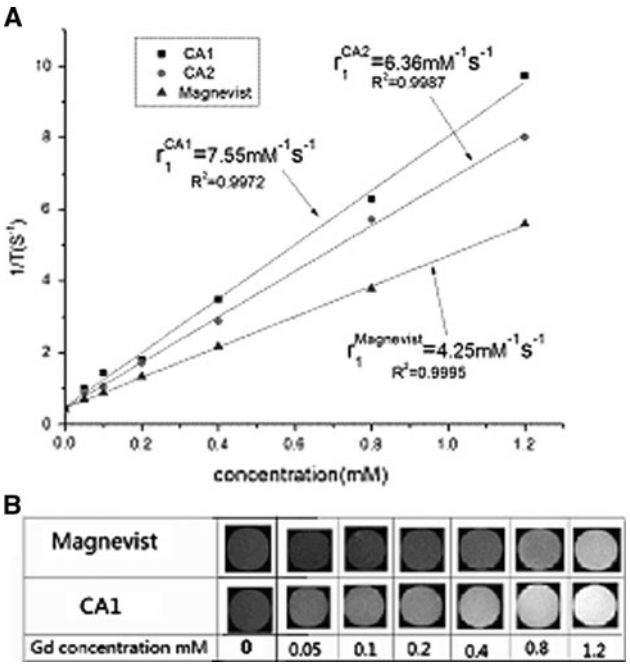

Fig. 5 **a** Longitudinal relaxation rate r_1, $1/T_1$ versus the concentration of gadolinium in aqueous solution at 11.7 T MRI spectrometer. **b** T_1-weighted spin-echo MR images in aqueous solution at 11.7 T MRI spectrometer

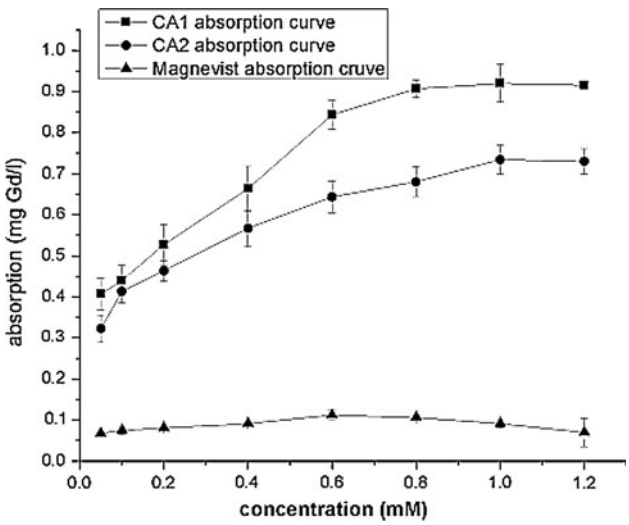

Fig. 6 Uptake quantity of CA1, CA2, and Magnvist in A549. Cultured A549 cells (5 × 105 cells/well) with CA1, CA21, and Magnevist for 8 h. Values represent mean ± SD of three independent experiments

partly block the uptake of **CA1** by A549. But **P1** included two targetable-tumor motifs of RGD and NGR can further block the uptake of **CA1** by A549 ($p < 0.01$, significant differences exist between group 1 and group 2, the same between group 1 and group 3). Figure 7b shows that cellular imaging without blocking reagent is much brighter than that with blocking reagent of **P1** or **P2**.

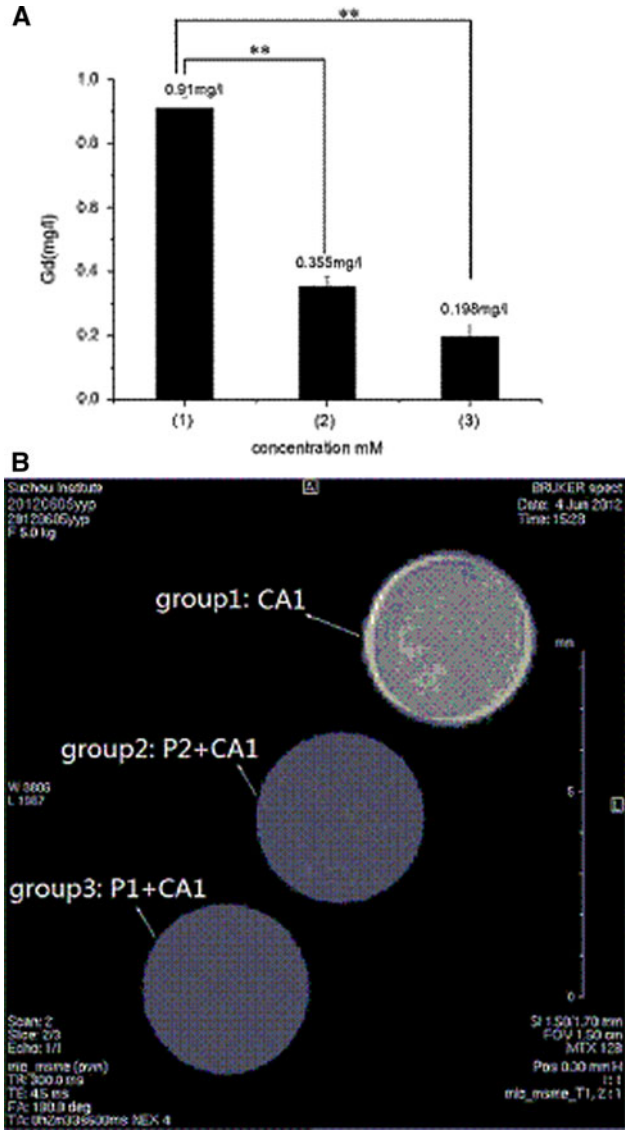

Fig. 7 **a** The result of competition binding (1) 0.8 mM **CA1**; (2) 0.8 mM P1+ 0.8 mM **CA1**; (3) 0.8 mM P2+ 0.8 mM **CA2**. The condition of culturing: first groups 2 and 3 were cultured in culture media at 37 °C for 2 h with addition of 0.8 mM **P1**, 0.8 mM **P2**, respectively. After that the three groups were cultured with 0.8 mM **CA1** in culture media for 8 h. Values represent mean ± SD of three independent experiments. (**$p < 0.01$, represents significantly different). **b** Cellular imaging results of competition binding in 11.7 T MRI spectrometer. Fixed the cells with 1 % agarose

Discussion

$\alpha_v\beta_3$ and CD_{13} have been recognized as tumor molecular markers and potential therapeutic targets. The two tumor-homing motifs of RGD and NGR can specifically bind to $\alpha_v\beta_3$ and CD_{13}, respectively. A lot of applications of molecular imaging and tumor therapeutic based on RGD/$\alpha_v\beta_3$ targeting delivery system have been reported (Dijkgraaf et al. 2007; Johanna et al. 2009). NGR/CD_{13}-based targeting delivery system is frequently reported in drug design used for cancer treatment (Wang et al. 2011; Albrecht et al. 2011), also reported using as imaging system (Soudy et al. 2012; Negussie et al. 2010). Taking notice of limited number of $\alpha_v\beta_3$ or CD_{13} that could be available, we designed and synthesized the contrast agent CA1 which contained two target-specific moieties of RGD and NGR. The design is very beneficial to $\alpha_v\beta_3$ and CD_{13} positive tumor cells such as A549. So far, there are no reports on this design.

The cyclic peptide is much more stable than their linear counterparts (Enwerem et al. 2012). Dathe et al. (2004) have reported that cyclic peptide improves the binding affinity to their cellular targets by minimizing the entropy cost of binding. Colomb and coworkers have demonstrated that the use of disulfide-bridged cyclic NGR peptide led to a tenfold increase in the efficacy of targeting to tumor sites compared with its linear analog (Colombo et al. 2002). So we linked the two Cys by disulfide bridge to improve the stability and the binding affinity. The synthesis processes of peptides and ligands were completed on the solid resin substrate. A solid-phase synthesis offers many advantages such as high coupling efficiency and convenient purification procedures. The various impurities and the excess reaction substances are easily removed from the reaction system simply by washing with appropriate solvent. The gadolinium complex was prepared by adding 0.99 equivalents of gadolinium chloride to a solution of ligand in water. A slight excess of ligand was used to ensure the absence of free gadolinium, which is highly toxic.

For MRI contrast agent, the relaxivity is a key performance, the higher relaxivity means better effect of imaging. Research shows that the bigger the molecular weight of the same series contrast agent the higher the relaxivity is higher; so the effect of imaging is better. From Fig. 5a, the longitudinal relaxivity of three contrast agent is $r_1^{CA1} > r_1^{CA2} > r_{1,}^{Magnevist}$ agreeing with the conclusion that increasing the molecular weight was beneficial to the improvement of the longitudinal relaxivity. The imaging of aqueous solution of **CA1** is brighter than that of Magnevist at the same concentration. **CA1** has good effect even at low concentrations. It is further seen

that the higher the relaxivity the better the imaging effect.

At the same concentration, the quantity of the three contrast agents absorbed by A549 shows the relationship of **CA1** > **CA1** > Magnevist, which demonstrate the binary targeting contrast agent **CA1** can target better the A549 cells than the single targeting contrast agent **CA2**, and the single targeting contrast agent **CA2** has better targeting effect than non-targeting Magnevist. The experiment results attest effectiveness and usefulness of the binary contrast agent designed by us. The uptake saturability can be reached, which can illustrate that the expression of $\alpha_v\beta_3$ and CD_{13} in A549 is limited, and can also indirectly demonstrate that, compared with the multimer of RGD or NGR, the assembly of RGD and NGR will lead to more effective absorption. The quantity of Magnevist absorbed by A549 was very low at all experiment concentrations because it is a nonspecific contrast agent. The difference of uptake quantity displays obviously that the binary targeting contrast agent **CA1** designed by us has better effect in targeting A549.

Using the peptide **P2** as the blocking agent partly blocked the incorporation of **CA1** and A549, and using the peptide **P1** as the blocking agent resulted in almost complete blockage of A549 uptake; the absorption quantity is equivalent to that of the nontargeting contrast agent Magnevist at the same concentration. Due to the impact of the blocking agent the cellular imaging is darker than the cellular imaging incubated with **CA1** in the absence of blocking agent. The results prove that **CA1** can bind specificity to the $\alpha_v\beta_3$ and CD_{13} of the surface of A549 cells.

Conclusion

In this study, we designed and synthesized a based-peptide binary tumor-targeted contrast agent **CA1**, determined its relaxivity, and evaluated its binding efficiency to A549 cells. The results show that **CA1** has higher relaxivity and can combine specifically with two tumor markers of $\alpha_v\beta_3$ and CD_{13}. Two targeting moieties result in higher concentration of the contrast agent to the surface of the tumor and better imaging effect. The experimental data warrant that simultaneous utilization of RGD and cNGR peptide as a tumor targeting moiety has been considered as a very promising strategy.

Acknowledgments The work was funded by the National Natural Science Foundation of China (No. 20675033, 20672039). The authors thank Center of Analysis and test, Huazhong University of Science and Technology (Wuhan, China) for assistance with ESI-MS and RP-HPLC analysis. The authors thank Division of Nanobionics, Suzhou Institute of Nanotech and Nanobionics, Chinese Academy of Sciences (Suzhou, China) for assistance with relaxivity measurements and phantom experiment.

Conflict of interest We declare that we have no financial and personal relationships with other people or organizations that can inappropriately influence our work and that there is no professional or other personal interest of any nature or kind in any product, service and/or company that could be construed as influencing the position presented in the manuscript.

References

Albrecht S, Al-Lakkis-Wehbe M, Orsini A et al (2011) Aminobenzosuberone: a novel warhead for selective inhibition of human aminopeptidase-N/CD13. Bioorg Med Chem 19:1434–1449

Caravan p (2009) Protein-targeted gadolinium-based magnetic resonance imaging (MRI) contrast agents: design and mechanism of action. Acc Chem Res 42:851–862

Colombo G, Curnis F, De Mori GMS, Gasparri A et al (2002) Structure-activity relationships of linear and cyclic peptides containing the NGR tumor-homing motif. J Biol Chem 277:47891–47897

Conradi J, Huber S, Gaus K et al (2012) Cyclic RGD peptides interfere with binding of the Helicobacter pylori protein CagL to integrins αvβ3 and α5β1. Amino Acids 43:219–232

Dathe M, Nikolenko H, Klose J, Bienert M (2004) Cyclization increases the antimicrobial activity and selectivity of arginine- and tryptophan-containing hexapeptides. Biochemistry 43:9140–9150

De León-Rodríguez LM, Kovacs Z (2008) The synthesis and chelation chemistry of DOTA peptide conjugates. Bioconj Chem 19:391–402

Dijkgraaf I, Kruijtzer JAW, Frielink C, Corstens FHM, Oyen WJG, Liskamp RMJ, Boerman OC (2006) $\alpha_v\beta_3$ Integrin-targeting of intraperitoneally growing tumors with a radiolabeled RGD peptide. Int J Cancer 120:605–610

Dijkgraaf I, Kruijtzer JAW, Liu S, Soede AC, Oyen WJG, Corstens FHM, Liskamp RMJ, Boerman OC (2007) Improved targeting of the $\alpha_v\beta_3$ integrin by multimerisation of RGD peptides. Eur J Nucl Med Mol Imaging 34:267–273

Enwerem I, Wang J, Leszczynski J (2012) In search of active RGD peptides: theoretical study of hydrogen bonding in five-member ring cyclic-RGD isomers. Comput Theor Chem 998:141–147

Hersel U, Dahmen C, Kessler H (2003) RGD modified polymers: biomaterials for stimulated cell adhesion and beyond. Biomaterials 24:4385–4415

Heverhagen JT, Graser A, Fahr A, Müller R, Alfke H (2004) Encapsulation of gadobutrol in AVE-based liposomal carriers for MR detectability. Magn Reson Imaging 22:483–487

Huang Y, Cao BN, Yang XL, Zhang Q, Han XJ, Guo ZY (2013) Gd complexes of diethylenetriaminepentaacetic acid conjugates of low-molecular-weight chitosan oligosaccharide as a new liver-specific MRI contrast agent. Magn Reson Imaging 31:604–609

Johanna H, Iina L, Pauliina L et al (2009) ^{68}Ga-DOTA-RGD peptide: biodistribution and binding into atherosclerotic plaques in mice. Eur J Nucl Med Mol Imaging 36:2058–2067

Kates SA, Sole NA, Johnson CR et al (1993) A novel, convenient, 3-dimensional orthogonal strategy for solid-phase synthesis of cycli c-peptides. Tetrahedron Lett 34:1549–1552

Langereis S, Dirksen S, De Waal BFM, Van Genderen MHP, De Lussanet QG, Hackeng TM, Meijer EW (2005) Solid-phase synthesis of a cyclic NGR-functionalized Gd^{III} DTPA complex. Eur J Org Chem 12:2534–38

Langereis S, Dirksen A, Hackeng TM, van Genderena MHP, Meijer EW (2007) Dendrimers and magnetic resonance imaging. New J Chem 31:1152–1160

Li ZJ, Cho CH (2012) Peptides as targeting probes against tumor vasculature for diagnosis and drug delivery. J Transl Med 10(Suppl 1):S1–S9

Liu Z, Niu G, Shi J, Liu S, Wang F, Liu S, Chen X (2009) ^{68}Ga-labeled cyclic RGD dimers with Gly3 and PEG4 linkers: promising agents for tumor integrin $\alpha_v\beta_3$ PET imaging. Eur J Nucl Med Mol Imaging 36:947–957

Ma W, Kang F, Wang Z et al (2013) 99mTc-labeled monomeric and dimeric NGR peptides for SPECT imaging of CD13 receptor in tumor-bearing mice. Amino Acids. doi:10.1007/s00726-013-1469-1

Mishra R, Su W, Pohmann R, Pfeuffer J, Sauer MG, Ugurbil K, Engelmann J (2009) Cell-penetrating peptides and peptide nucleic acid-coupled MRI contrast agents: evaluation of cellular delivery and target binding. Bioconj Chem 20:1860–1868

Ndinguri MW, Solipuram R, Gambrell RP, Aggarwal S, Hammer RP (2009) Peptide targeting of platinum anti-cancer drugs. Bioconj Chem 20:1869–1878

Negussie AH, Miller JL, Reddy G et al (2010) Synthesis and in vitro evaluation of cyclic NGR peptide targeted thermally sensitive liposome. J Control Release: Off J Control Release Soc 143:265–273

Nwe K, Bryant LH Jr, Brechbiel MW (2010) Poly(amidoamine) dendrimer based MRI contrast agents exhib enhanced relaxivities derived via metal preligation techniques. Bioconj Chem 21:1014–1017

Sarin VK, Kent SBH, Tam JP et al (1981) Quantitative monitoring of solid-phase peptide synthesis by the ninhydrin reaction. Anal Biochem 117:147–157

Schroeder RPJ, Weerden WM, Krenning EP, Bangma CH, Berndsen S, Grievink-de Ligt CH, Groen HC, Reneman S, de Blois E, Breeman WAP, de Jong M (2011) Gastrin-releasing peptide receptor-based targeting using bombesin analogues is superior to metabolism-based targeting using choline for in vivo imaging of human prostate cancer xenografts. Eur J Nucl Med Mol Imaging 38:1257–1266

Seward GK, Qian W, Dmochowski IJ (2008) Peptide-mediated cellular uptake of cryptophane. Bioconj Chem 19:2129–2135

Soudy R, Ahmed S, Kaur K (2012) NGR peptide ligands for targeting CD13/APN identified through peptide array screening resemble fibronectin sequences. ACS Comb Sci 14:590–599

Wang RYE, Niu YH, Wu HF, Amin MN, Cai JF (2011) Development of NGR peptide-based agents for tumor imaging. Am J Nucl Med Mol Imaging 1(1):36–46

Ye FR, Jeong EK, Jia ZJ, Yang TX, Parker D, Lu ZR (2008) A Peptide targeted contrast agent specific to fibrin-fibronectin complexes for cancer molecular imaging with MRI. Bioconj Chem 19:2300–2303